DOI: 10.1002/ejic.200900136

# Experimental and Theoretical Evidence of π-d Interactions in Supramolecular Assemblies Based on TTF-CH=CH-Py Ligands Tethered to $Mo_6X^i_8$ Octahedral Molybdenum Halide Cluster Cores

**Ganesan Prabusankar,[a] Yann Molard,*[a] Stéphane Cordier,*[a] Stéphane Golhen,*[a] Yann Le Gal,[a] Christiane Perrin,[a] Lahcène Ouahab,*[a] Samia Kahlal,[a] and Jean-François Halet*[a]**

**Keywords:** Molybdenum / Cluster compounds / Early transition metals / Ligands / Supramolecular chemistry / Charge transfer

Synthesis, characterization, and physical properties of $[Mo_6X^i_8(TTF\text{-}CH{=}CH\text{-}Py)^a_6]^{4+}$ supramolecular assemblies [TTF = tetrathiafulvalene; Py = pyridine; X = Cl (**1**), Br (**2**), I (**3**)] resulting from the reaction between $[Mo_6X^i_8(OSO_2CF_3)_6]^{2-}$ cluster precursor and TTF-CH=CH-Py ligands were investigated. They are based on the association of the strongly delocalized metallic electron $[Mo_6X^i_8]^{4+}$ cluster cores with six redox-active π-conjugated TTF-CH=CH-Py terminal ligands attached to the Mo clusters through the pyridinyl group. Synergetic π-d interactions between the organic ligands and the cluster core were experimentally evidenced by electrochemistry and absorption measurements, and corroborated by DFT calculations.



## Introduction

Today organic–inorganic hybrid materials constitute an active area of research at the forefront of solid-state science.[1] In this area, soluble, molecular forms of inorganic transition-metal clusters have begun to be employed as building units in the construction of hybrid extended solid frameworks or supramolecular assemblies.[2] The 24 metal-valence-electron (MVE) $[Mo_6X^i_8X^a_6]^{2-}$ octahedral anionic cluster units [$X^i$ = inner (face-bridged), $X^a$ = apical, X = Cl, Br, I] obtained by the solid-state chemistry route, and based on a rigid $Mo_6X^i_8$ cluster core additionally bonded to six apical ligands ($X^a$)[3], are good candidates for this purpose. They can be used as soluble building blocks either directly[4] or after functionalization for the synthesis of various hybrid architectures including dendrimers and extended molecular arrays.[5] Indeed, the apical halogen ligands are semilabile and can be replaced in solution by donor ligands to lead to various functional $[Mo_6X^i_8L^a_6]^{n+/-}$ cluster units (L = $PR_3$, pyridine derivatives...), which have been studied over the years.[5] As organic functional ligands, tetrathiafulvalene (TTF) derivatives serve as a successful class of electroactive and/or magnetic organic moieties for the preparation of hybrid materials. In this respect, TTF and its derivatives have been widely used as electron donor components in the preparation of charge-transfer (CT) complexes and radical ion salts, which exhibit interesting conducting and magnetic behaviors.[6] Furthermore, TTF derivatives bearing coordination functions such as pyridine[7,8] are well known for their ability to coordinate to transition-metal ions. Mononuclear and polynuclear paramagnetic transition-metal fragments coordinated to these redox-active ligands through coordination functions have already been prepared and investigated.[9] Although many examples of molecular assemblies based on the $[Mo_6X_8]^{4+}$ core and pyridine derivative ligands are reported in the literature,[4] to the best of our knowledge there has been no report so far on the association of $Mo_6$ clusters with TTF/pyridine ligands. The coordination by covalent bonding of TTF-based ligands to the molybdenum clusters through pyridine (Py) linkage should constitute an extremely interesting class of organic–inorganic hybrid cations, combining the advantages and properties of TTF-based materials (π-stacking self-assembling, magnetism, electronic charge transfer) with those of inorganic clusters (magnetism, luminescence, electronic properties) with possible synergetic effects. Of particular interest is the TTF-CH=CH-Py (**L1**) ligand, in which the TTF and pyridine moieties are linked by an ethyl-

[a] Unité Sciences Chimiques de Rennes, Université de Rennes 1, UMR CNRS 6226,
Campus de Beaulieu, Avenue du Général Leclerc, 35042 Rennes, France
Fax: +33-2-23236799
E-mail: stephane.cordier@univ-rennes1.fr
stephane.golhen@univ-rennes1.fr
halet@univ-rennes1.fr
yann.molard@univ-rennes1.fr
ouahab@univ-rennes1.fr

Supporting information for this article is available on the WWW under http://www.eurjic.org or from the author.

  

ene bridge. **L1** is expected to coordinate the $Mo_6$ cluster through the pyridinyl group, which should favor electronic communication between TTF and the $Mo_6$ cluster and bring the organic π system closer to the metal centers.

We report here the synthesis and detailed investigations of $[Mo_6X^i_8(TTF\text{-}CH{=}CH\text{-}Py)_6]^{4+}$ supramolecular assemblies [X = Cl (**1**), Br (**2**), I (**3**)] built up from the association of the inorganic $Mo_6$ transition-metal cluster core with the π-conjugated TTF-based organic ligand **L1**. Synergetic π-d interactions between the ligands and the cluster core are evidenced. Results are then compared with those found in the literature for relevant related compounds or complexes.

## Results and Discussion

### Synthesis

Scheme 1 illustrates the experimental procedure used for the synthesis of the $[Mo_6X^i_8(\mathbf{L1})^a_6]^{4+}$ complexes (X = Cl, Br, I). The $[(n\text{-}C_4H_9)_4N]_2Mo_6X^i_8X^a_6$ precursors were prepared from $Cs_2Mo_6X^i_8X^a_6$ inorganic ternaries by cationic metathesis according to the procedure reported in the literature.[10] Crystalline $[(n\text{-}C_4H_9)_4N]_2[Mo_6X_8(OSO_2CF_3)_6]$ (X = Cl, Br, I) intermediates were easily obtained from $[(n\text{-}C_4H_9)_4N]_2[Mo_6X^i_8X^a_6]$ by reaction with $AgSO_3CF_3$ in organic media in order to replace apical halogen by $SO_3CF_3$ labile groups, as previously reported in the literature.[11] Then, the $Mo_6X^i_8$ cluster cores were functionalized by the reaction of $[(n\text{-}C_4H_9)_4N]_2[Mo_6X_8(OSO_2CF_3)_6]$ with a slight excess of **L1**[12] in THF. An immediate color change from yellow to violet upon addition of ligands to the cluster solution indicated the exchange of triflate anions. However, the mixture was stirred for 5 d at 80 °C to fully complete the reaction.

The identities of the compounds were confirmed by $^1H$ NMR spectroscopy. Full assignment of NMR spectra were realized using $^{13}C\{^1H\}$ HMBC, HSQC, and $^{15}N\{^1H\}$ HMBC NMR spectroscopy experiments in $CD_3COCD_3$. The $^{19}F$ NMR indicates that the upfield shift of the $-CF_3$ signal of the triflate moieties moves from –73 ppm in the triflate precursors $[(n\text{-}C_4H_9)N]_2[Mo_6X_8(OSO_2CF_3)_6]$ to –79 ppm in $[Mo_6X_8(\mathbf{L1})_6](OSO_2CF_3)_4$. The difference has been attributed to the different roles, coordinated ligand or counteranion, of the triflate moiety in the $[Mo_6X_8(OSO_2CF_3)_6]^{2-}$ anionic unit and for the $[Mo_6X_8(\mathbf{L1})_6]^{4+}$ cationic complex, respectively.

To confirm the binding of the ligand through the nitrogen atom of the pyridine group onto the ionic cluster cores, $^{15}N\{^1H\}$ HMBC NMR experiments were carried out in $CD_3COCD_3$ for **L1** and **1**–**3**. In all cases a single resonance associated to the pyridine nitrogen atom in **1**–**3** was detected, attesting the disappearance of the tetrabutylammonium cation of the $[Mo_6X_8(OSO_2CF_3)_6]^{2-}$ intermediate in the media. Moreover, drastic upfield shifts of about 120 ppm from –62.5 ppm for **L1** to –180 ppm for **1** and –183 ppm for **2** and **3** were observed, showing an increase of the electronic density on the nitrogen atom induced by the ligand anchoring onto the cluster by the pyridine. Figure 1 shows the $^1H$ NMR spectra of the free ligand **L1** and the three complexes **1**–**3** in $CD_3COCD_3$.

Comparison of the $^1H$ spectra of the free ligand and of the modified clusters reveals several changes in the chemical shifts of the ligand proton signals upon complexation. Because of the complete conjugation of the ligand, its complexation onto the cluster core induces changes in the overall $^1H$ NMR spectrum. The complexation induces large downfield shifts of the signals corresponding to the pyridinyl and the ethenyl protons. For example, in the case of compound **1**, those protons signals are deshielded from $\delta$ = 8.55 to 8.97 ppm for $H_a$, from $\delta$ = 7.49 to 8.32 ppm for $H_b$, from $\delta$ = 6.44 to 6.70 ppm for $H_c$, and from $\delta$ = 7.46 to 7.97 ppm for $H_d$. The two proton signals of the TTF moiety are also affected by the complexation, but a greater effect is observed for $H_e$ than for $H_f$.

A closer inspection of the aromatic region of the $^1H$ NMR spectra of **1**, **2**, and **3** suggests a small influence of the nature of the inner ligands on the chemical shifts of the pyridinyl and ethenyl protons that are slightly more deshielded from X = I to X = Cl (see Supporting Information).

$^{13}C\{^1H\}$ HMBC and HMQC experiments were used to assign all the $^{13}C$ chemical shifts to their respective carbon atoms. As recently described by Pazderski and co-workers in the case of pyridine coordinated to various transition-metal cations,[13] for the majority of carbon atoms, the complexation induces a moderate deshielding effect up to 11.4 ppm. But surprisingly, the cluster coordination results

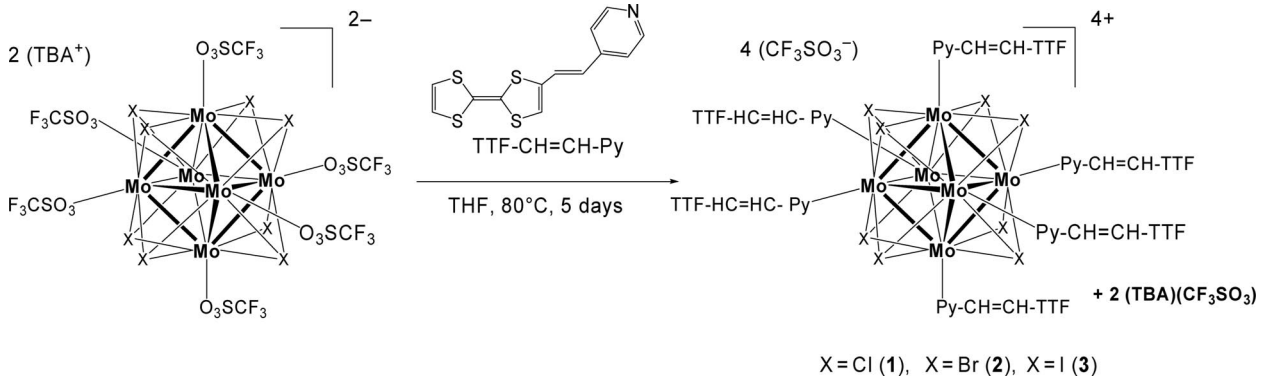


Scheme 1. Synthesis of complexes **1**, **2**, and **3**. TBA = tetrabutylammonium $[(n\text{-}C_4H_9)_4N^+]$.

  

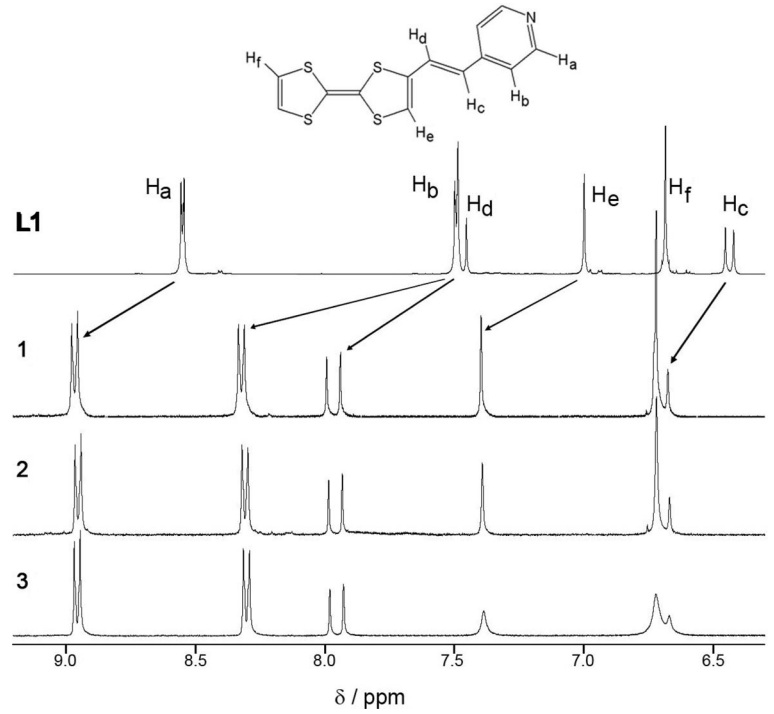


Figure 1. $^1$H NMR spectra of **1**–**3** in $CD_3COCD_3$.

also in a large shielding of the two carbon atoms located in the α position of the nitrogen atom ($\Delta\delta$ = –8.2 ppm for **1**, –8.5 ppm for **2**, and –8.4 ppm for **3**). As the intramolecular charge transfer (CT) capability of TTF towards pyridine through a conjugated bond has been well established,[14] this unexpected result may be due to the electron-accepting ability of the pyridinyl group that is enhanced by complexation[15] as well as to π-backbonding from the cluster to **L1**. From NMR results, it can be seen that the TTF moiety is positively charged and the N, C2, and C3 atoms from pyridine exhibit an excess of electrons.

Unfortunately, single crystals of sufficient quality could not be grown for compounds **1**–**3**. The utility of density functional theory (DFT) calculations has been previously demonstrated for calculating, with good confidence, geometries of molecules for which X-ray data are not available. Therefore, DFT calculations were carried out on $[Mo_6Cl_8(\mathbf{L1})_6]^{4+}$ (**1**). A drawing of the optimized geometry is shown in Figure 2. A complete list of the calculated bond lengths for a molecule containing an omnicapped octahedral $[Mo_6Cl_8]^{4+}$ core bearing six terminal **L1** ligands is given in Table 1 (see Figure 3 for the atom numbering in **L1**). Optimization showed that **L1** is not planar and that the pyridine does not lie in the $Mo_4$ planes.

With average Mo–Mo and Mo–$Cl^i$ distances of 2.687 and 2.562 Å, respectively, the structure of the $[Mo_6Cl_8]^{4+}$ core is essentially identical to that found in other compounds containing this kind of chloridomolybdenum cluster. For instance, Mo–Mo and Mo–$Cl^i$ distances of 2.689 and 2.561 Å, respectively, are computed for $[Mo_6Cl^i{}_8Cl^a{}_6]^{2-}$. (*Note:* a deviation of about 0.1 Å is observed between the computed and experimental distances. Nonlocal

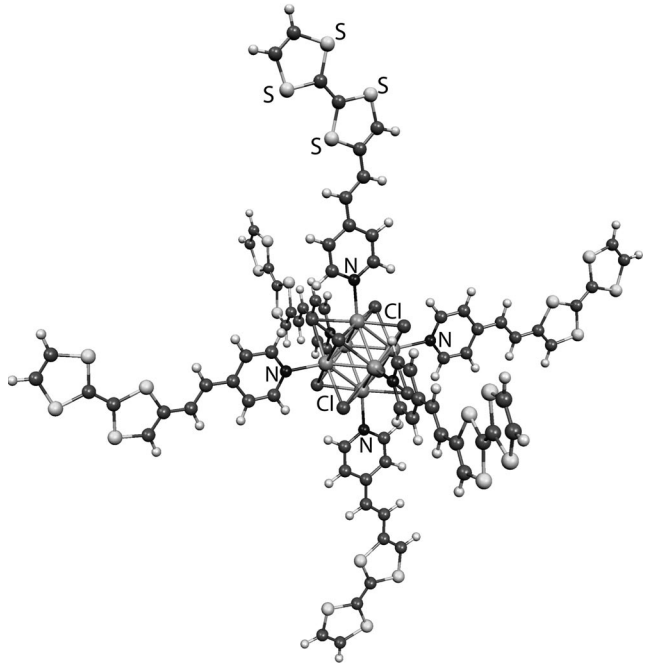


Figure 2. Optimized geometry of complex **1**.

corrected DFT computations show a tendency to overestimate bond lengths.) Average Mo–N bonding distances of 2.218 Å are computed. They are slightly shorter than Mo–N(Py) distances (av. 2.25 Å) measured in $[(\eta^5\text{-}C_6H_5CH_3)\text{-}Mo(Py)_3][B(C_6H_5)_4]$ for instance.[16] Main bonding distances in the attached nearly planar **L1** ligands are comparable to those computed for the free ligand and those experimentally measured in the closely related 1-methyl-4-[2-

  

Table 1. HOMO–LUMO gaps [eV] and computed interatomic distances [Å] for TTF-CH=CH-Py (**L1**), $[Mo_6Cl_8(TTF\text{-}CH{=}CH\text{-}Py)_6]^{4+}$ (**1**), and $[Mo_6Cl^i{}_8Cl^a{}_6]^{2-}$ ($^i$ inner, $^a$ apical; the atom numbering of **L1** is depicted in Figure 3).

| | **L1** ($C_s$) | **1** ($C_1$) | $[Mo_6Cl_8(Cl)_6]^{2-}$ ($O_h$) |
|---|---|---|---|
| HOMO–LUMO gap / eV | 1.355 | 0.21 | 2.39 |
| Mo–Mo range | | 2.674–2.699 | 2.689 |
| Mo–Mo average | | 2.687 | |
| Mo–N range | | 2.208–2.227 | |
| Mo–N average | | 2.218 | |
| Mo–$Cl^i$ range | | 2.560–2.565 | 2.561 |
| Mo–$Cl^i$ average | | 2.562 | |
| Mo–$Cl^a$ | | | 2.481 |
| N–C2 | 1.347 | 1.363–1.364 | |
| N–C3 | 1.344 | 1.363–1.364 | |
| C2–C4 | 1.392 | 1.373–1.374 | |
| C3–C5 | 1.394 | 1.372–1.373 | |
| C4–C6 | 1.411 | 1.419–1.420 | |
| C5–C6 | 1.409 | 1.416–1.417 | |
| C6–C7 | 1.458 | 1.424–1.426 | |
| C7–C8 | 1.358 | 1.370–1.372 | |
| C8–C9 | 1.436 | 1.415–1.417 | |
| C9–C10 | 1.361 | 1.372–1.374 | |
| C9–S11 | 1.784 | 1.782–1.783 | |
| C10–S12 | 1.736 | 1.703–1.705 | |
| S11–C13 | 1.780 | 1.771–1.773 | |
| S12–C13 | 1.777 | 1.752–1.753 | |
| C13–C14 | 1.360 | 1.376–1.377 | |
| C14–S15 | 1.781 | 1.761 | |
| C14–S16 | 1.781 | 1.761 | |
| S15–C17 | 1.757 | 1.746 | |
| S16–C18 | 1.757 | 1.745 | |
| C17–C18 | 1.343 | 1.342 | |

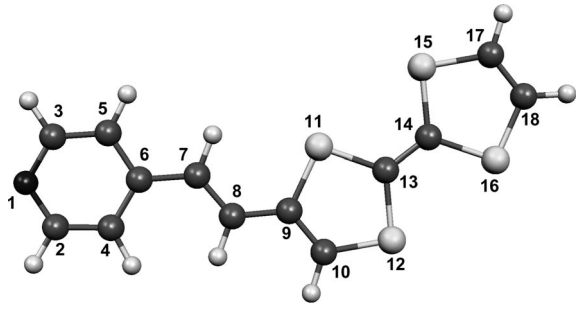


Figure 3. Representation of TTF-CH=CH-Py (**L1**) and atom numbering.

(tetrathiafulvalenyl)ethenyl]pyridinium iodide compound.[12] For instance the C–C bond of the ethenyl group is 1.371 Å, slightly longer than the corresponding distance in free **L1**, which is 1.358 Å. Inside the TTF part, the central C–C, and outside C–C and C–S bonds are 1.377 (av.), 1.358 (av.), and 1.752 (av.) Å, respectively, compared to 1.360 (av.), 1.352 (av.), and 1.768 (av.) Å, respectively, in the free neutral ligand. Some charge transfer from the TTF-π-spacer-acceptor ligands **L1** to the cluster $[Mo_6Cl_8]^{4+}$ core is reflected in the slight change of the bond lengths, that is, some lengthening of the central C–C bond and some shortening of the C–S bonds in the TTF moiety. Moreover, this slight change in distances indicates that the TTF moiety is not neutral but rather positively charged when coordinated. On the basis of these calculations, we assume that the structural arrangement of compounds **2** and **3** is similar.

## Electronic Structure

The molecular orbital (MO) energy-level diagram of compound **1** is given in Figure 4 for the HOMO–LUMO region. A comparison with the MO diagram of the free **L1** ligand recalled in Figure 5 indicates that cluster-based MOs intercalate between ligand-based occupied and vacant MOs. Indeed, the six HOMOs of **1** derive almost exclusively from the HOMO (7a′′) of the **L1** ligand, which is localized on the TTF moiety. The next 12 occupied MOs also descend from the organic ligand (6a′′ and 5a′′ MOs). The next two occupied MOs are cluster in character and resemble the $e_g$ set, that is, the HOMO of any 24-MVE halogen octahedral cluster.[17]

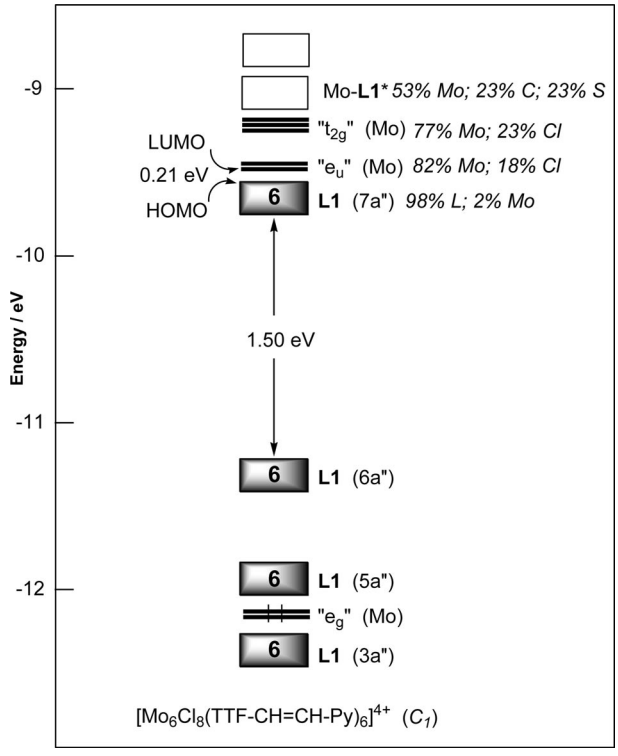


Figure 4. Frontier molecular orbital energy diagram of complex **1**. Symmetry labels in brackets correspond to MOs of isolated **L1** (Figure 5).

The LUMOs of the free ligand are mainly localized on the π-spacer and the pyridinyl part and lie at rather high energy. Some interactions with cluster MOs pushes them up in energy and they become largely separated from the HOMOs in **1**. Weakly perturbed cluster MOs are inserted in between and become the LUMOs of **1**, "$e_u$" and "$t_{2g}$" in Figure 4. A HOMO–LUMO gap of 0.21 eV is then computed, considerably smaller than 1.36 eV computed for the free ligand **L1**, and 2.39 eV for $[Mo_6Cl^i{}_8Cl^a{}_6]^{2-}$.

  

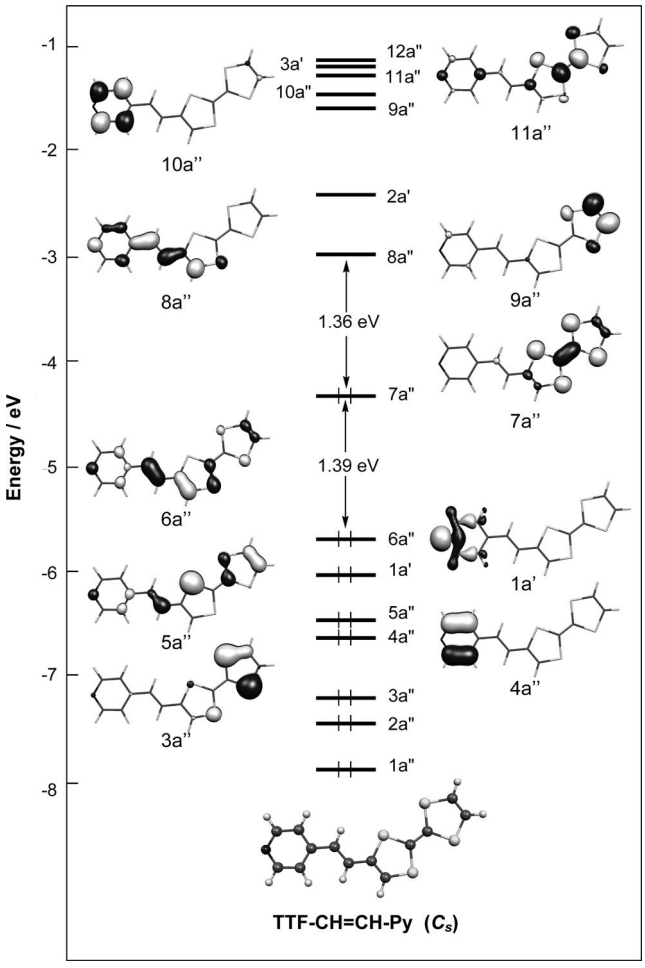


Figure 5. Frontier molecular orbital energy diagram of the free ligand **L1**.

The charge transfer from the TTF-π-spacer-acceptor ligands **L1** to the cluster $[Mo_6Cl_8]^{4+}$ core mentioned above on the basis of the change of bond lengths in the ligand is also reflected in the Mulliken computed fragment net charges, which are +1.87 and +2.13 (i.e., +0.36 per **L1**) for the $Mo_6Cl_8$ cluster core and the six terminal ligands, respectively. For comparison, the charge computed for $[Mo_6Cl^i_8Cl^a_6]^{2-}$ cluster units are +1.06 and –3.06 for the $Mo_6Cl^i_8$ cluster core and six $Cl^a$ ligands, respectively.

## UV/Vis Spectroscopy

Absorption spectroscopy measurements were carried out on compounds **1**–**3** in THF (Figure 6) and acetonitrile. No solvatochromic effect was detected on freshly prepared samples. However, a decomplexation process in acetonitrile after 48 h under inert atmosphere was evidenced by the growth of the uncomplexed ligand absorption band. This shows its release in solution and therefore its suspected replacement by solvent molecules in the coordination sphere of the cluster cation. Air bubbling into freshly prepared solutions of complexes also induced decomplexation of ligands, thus showing air and moisture sensitivity. Therefore, sample solutions in freshly distilled and degassed THF were prepared under inert atmosphere in an argon-filled glovebox shortly prior to use. In order to evaluate the influence of the coordination on the electronic properties of the ligand and the cluster core, the spectra of the ligand **L1** and the $[(n\text{-}C_4H_9)N]_2[Mo_6Cl_8(OSO_2CF_3)_6]$ starting precursor were also studied. They are shown in Figure 6 (b) along with the spectrum of **1**. The molar absorption coefficients of the ligand were multiplied by six with respect to the number of ligands around the cluster core in the complexes.

Compounds **1**–**3** exhibit rather intense absorption bands in the near-UV and visible regions. No significant changes due to the nature of the inner ligand were observed. The absorption spectrum of the free ligand **L1** shows two bands: one intense band with a maximum at 302 nm and a less intense one at 450 nm. Relevant to these experimental absorption bands, the time-dependent (TD) DFT-computed absorption spectrum of **L1** indicates an intense band at 326 nm (oscillator strength $f = 0.68$) and a less intense band at 367 nm ($f = 0.35$). Both bands result from a mixture of electronic transitions that arise mainly from low-lying π-type TTF-based MOs: 5a′′ for the intense band and 6a′′ for the less intense band (Figure 5) to the pyridinyl-based LUMO (8a′′) and from the TTF-based HOMO (7a′′) to

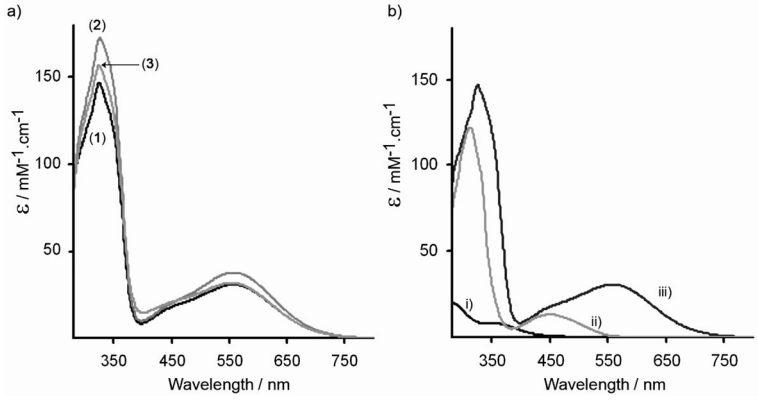


Figure 6. Absorption spectra obtained in THF for (a) complexes **1**, **2**, and **3**; (b) (i) $[(n\text{-}C_4H_9)N]_2[Mo_6Cl_8(OSO_2CF_3)_6]$, (ii) six ligands **L1**, (iii) complex **1**.

  

high-lying TTF-based MOs (12a′′ and 11a′′). Note that a weak band corresponding to the HOMO–LUMO transition is computed on the far right of the visible region at 789 nm ($f$ = 0.10).

The anchorage of the ligands onto the cluster core leads to a new band at 560 nm for **1** and **2** and 554 nm for **3**. Indeed, resulting complexes show a dark violet color, while the free ligand and the cluster precursors are yellow solids. Because of the size of the molecules, electronic transitions in the UV/Vis region for **1** could not be computed. Nevertheless, intercalation of cluster-based MOs between the HOMO and LUMO of the ligands in the complexes (Figure 4) might lead to new bands involving ligand-based or cluster-based MO to cluster-based MO transitions. Such transitions are not observed in this region for $[Mo_6Cl^i_8Cl^a_6]^{2-}$.[18]

Moreover, as illustrated in Figure 6 (b) in the case of complex **1**, all three complexes absorb much more strongly than either the triflate-substituted cluster or the free ligand, even when corrected for the presence of the six ligands per complex. This can be explained by an intensity-stealing mechanism brought about by vibronic coupling between the **L1** charge-transfer bands and $[Mo_6X^i_8]^{4+}$ cluster-based transitions, as observed by Shriver and co-workers in the case of redox-active ferrocenecarboxylate[19] or electron-rich cyanide complexes[20] grafted onto $[Mo_6Cl^i_8]^{4+}$.

With a small redshift, the absorption spectrum of **L1** is moderately affected in the M·**L1** complex series when M = $Cd^{2+}$, $Zn^{2+}$, alkali, or alkaline earth cations. Surprisingly enough, a larger perturbation is observed when M = $Pb^{2+}$.[7m] According to the authors, the redshift that is noted upon metal addition must be attributed to a peculiar ligand/cation interaction leading to a decrease of the energy of the LUMO level of the pyridinyl group because of an increase of its electron-accepting ability upon interaction with the $Pb^{2+}$ cation. Note that the intensity-stealing mechanism mentioned earlier for compounds **1**–**3** was not observed for $Pb^{2+}$·**L1**. Obviously, different interactions (i.e., appearance of a new CT band along with intensity-stealing mechanism) between $Mo_6$ and **L1** are at work in compounds **1**–**3**.

### Electrochemistry

Table 2 summarizes the oxidation potentials measured for TTF, **L1**, and complexes **1**–**3**. As shown in Figure 7, the cyclic voltammogram of the free ligand **L1** exhibits two oxidation waves, $E_1$ = 0.63 V and $E_2$ = 0.92 V (vs. SCE), assigned to the generation of the monoradical cation ($TTF^{+\cdot}$) and dication ($TTF^{2+}$). For comparison, the oxidation potentials of TTF in THF are $E_1$ = 0.596 V and $E_2$ = 0.896 V (vs. SCE). The increased potentials in **L1** compared to those of TTF are due to some electron transfer from TTF to Py by the CH=CH bridges leading to a decrease and increase of the electronic densities on the TTF and pyridine moieties, respectively. Surprisingly, when **L1** is coordinated to the $Mo_6X^i_8$ cluster core, $E_1$ and $E_2$ become significantly lower than for noncoordinated **L1** and even slightly lower than for nonsubstituted TTF [$E_1$ = 0.56 V and $E_2$ = 0.83 V (vs. SCE) for complex **1** for instance].

Table 2. Oxidation potentials vs. SCE [V] of TTF, **L1**, and **1**–**3** in THF.[a]

| | TTF | L1 | 1 | 2 | 3 |
|---|---|---|---|---|---|
| $E_1$ | 0.596 | 0.63 | 0.56 | 0.57 | 0.55 |
| $E_2$ | 0.896 | 0.92 | 0.83 | 0.78 | 0.80 |

[a] In THF-$Bu_4NPF_6$ (0.1 M), scan rate: 100 mV·s$^{-1}$; reference electrode: SCE; working electrode and counterelectrode: Pt.

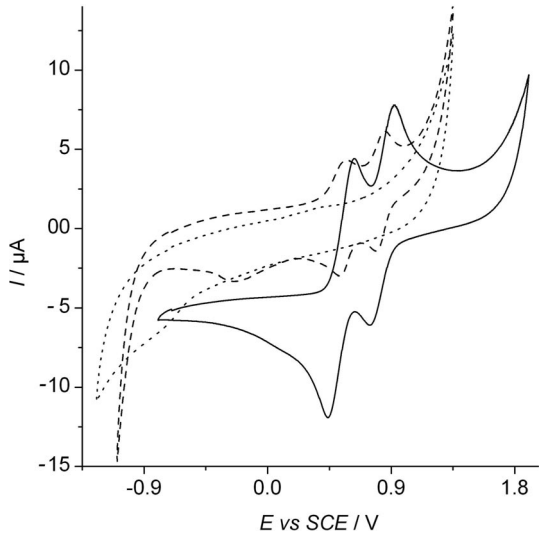


Figure 7. Cyclic voltammograms of the free ligand **L1** (plain line), $[(n\text{-}C_4H_9)N]_2[Mo_6Br_8(OSO_2CF_3)_6]$ (dotted line), and complex **2** (dashed line).

This is a very important result, which indicates that some electronic density is back on the electron-accepting pyridinyl group upon complexation of **L1** by the $(Mo_6X^i_8)^{4+}$ cluster core. Consequently, less electron transfer occurs from the electron-donating TTF part to the Py moiety. The TTF part being more electron-rich, the HOMO of complexes **1**–**3**, heavily localized on TTF, rises somewhat in energy. This can also be explained in terms of a destabilization of the 7a′′ level of **L1** by metallic levels of the cluster core (Figures 4 and 5). This renders complexed **L1** easier to oxidize than before complexation. Note that the complexation of **L1** by $Pb^{2+}$ leads to the opposite, that is, a shift of the oxidation potentials to higher values[7m] ($E_1$ = 0.44 V and $E_2$ = 0.81 V for **L1**, and $E_1$ = 0.51 V and $E_2$ = 0.89 V for Pb; **L1** in $CH_3CN$). This reflects some increase in the electron-accepting ability of the pyridinyl group and some decrease of the electronic density on the TTF moiety (Table 2).

An interesting feature is that the cyclic voltammograms of $[(C_4H_9)_4N]_2Mo_6X^i_8(CF_3SO_3)^a_6$ (Figure 7) precursors display a high-potential irreversible reduction wave located at –0.79 V for X = Br (–0.89 V for X = I and –0.70 V for X = Cl) that is shifted about –0.25 V for **1**–**3**. Note that the cyclic voltammograms of the free moiety **L1** do not exhibit any reduction wave. Supposedly, according to the MO diagram of **1**, which indicates that the LUMOs are cluster-based (see above), reduction must occur on the cluster core,

  

Table 3. Oxidation potentials [V] of species related to cluster complexes.

| | Solvent | $TTF^+/TTF^{2+}$ | $E_1/E_2$ | Ref. |
|---|---|---|---|---|
| $(SbF_6)_2[Re_6Se_8((Me_2TTF)\ PPh_2)_6]$ | $CH_2Cl_2$ | 0.58/1.05 | 0.33/0.71 | [21b] |
| $(SbF_6)_2Re_6Se_8[(Me_2TTF)_2PPh]_6$ | $CH_2Cl_2$ | 0.60/1.02 | 0.38–0.49/0.90 | [21b] |
| $W_6S_8(PEt_2TTF)_6$ | $C_7H_5N$ | 0.50/0.93 | 0.45/0.87 | [21a] |

leading to an unstable 25-MVE species. The increase of the reduction potential from –0.9 V for the triflate $Mo_6$ cluster to –0.25 V in **1**–**3** is explained by some electron transfer from the cluster core to the pyridinyl part of the **L1** ligands, decreasing the electron-donor properties of the former.

Synthesis of $Re_6$ and $W_6$ octahedral clusters associated with TTF moieties but with a different spacer has been reported, for instance, for the 20-MVE $W_6S_8(PEt_2TTF)_6$[21a] and 24-MVE $(SbF_6)_2[Re_6Se_8(PPh_2(Me_2TTF))_6]$, and 24-MVE $(SbF_6)_2[Re_6Se_8(PPh(Me_2TTF)_2)_6]$[21b] species. Conversely to the electronic delocalization that can occur between the cluster and the **L1** ligands in complexes **1**–**3**, electronic delocalization between the π system of the TTF moiety and the cluster in these $Re_6$ and $W_6$ compounds is hardly expected owing to the $sp^3$ hybridization of phosphorus in the phosphane moieties. Electrovoltammetry studies performed on these complexes also exhibit two oxidation waves corresponding to the oxidation of TTF to $TTF^+$ and $TTF^{2+}$, respectively. Values are given and compared to those of the free ligands in the same solvent in Table 3. Unexpectedly, a cathodic shift larger than (or at least comparable to) those for complexes **1**–**3** is observed. In the 20-MVE species $W_6S_8(PEt_2TTF)_6$, for instance, the cyclic voltammogram in benzonitrile exhibits two reversible oxidation waves at potentials 0.05 V lower than the free ligand (Table 3). An irreversible reduction wave appears at –0.45 V for $W_6S_8(PEt_2TTF)_6$ and at –0.3 V for the free $PEt_2TTF$ ligand. Di Salvo et al. suspect some charge transfer in this compound between the phosphorus atom and TTF of the $PEt_2TTF$ ligands even though no lone pair remains on the former.[21a] They also suggest that the first potential could result from a contribution of both the $W_6$ cluster and the attached ligands, but no clear conclusion was drawn.[21a] However, in this $W_6$ cluster molecule, the number of electrons per cluster is 20 and the magic number of 24 is not reached. Consequently, metal–metal bonding orbitals or at least no bonding orbitals are available to receive an electron from reduction. Electron donation in the 24-MVE compounds $(SbF_6)_2[Re_6Se_8(PPh_2(Me_2TTF))_6]$ and $(SbF_6)_2[Re_6Se_8(PPh(Me_2TTF)_2)_6]$ from the cluster core to the TTF groups must be even more important, as a cathodic shift for the first and second oxidation potential of 0.22–0.25 V and 0.12–0.34 V, is measured, respectively.[21a] This can be explained by an important destabilization of the HOMO level of TTF-based ligands when they are coordinated to the cluster, as found here for **1**–**3**. Note that for the 24-MVE $Re_6$ complexes, no reduction wave has been reported, meaning a larger HOMO–LUMO energy gap in the whole $(SbF_6)_2[Re_6Se_8(PPh_2(Me_2TTF))_6]$ and $(SbF_6)_2[Re_6Se_8(PPh(Me_2TTF)_2)_6]$ complexes than in **1**–**3**.

## Conclusions

$[Mo_6X^i_8](\mathbf{L1})_6$ complexes [X = Cl, Br, I (**1**–**3**)] have been obtained by reaction of the $[Mo_6X^i_8](CF_3SO_3)^a_6$ cluster precursor with six **L1** ligands in which TTF and a pyridine moiety are bridged by an ethylene group, favoring electronic communication between the TTF groups and the cluster core. It turns out that the coordination of these ligands through the nitrogen atom of the pyridinyl moiety onto the six apical positions of the cluster has been evidenced by $^1H$ NMR with a drastic downfield shift of the pyridine proton signals and by $^{15}N$ NMR spectroscopy.

The linkage of the pyridine moiety to the cluster is accompanied by some charge transfer from the latter to the former. Consequently this diminishes its electron-accepting ability and thus the intramolecular charge transfer from the TTF part to the pyridine. This leads to some energy destabilization of the TTF-based HOMO, which is reflected in a redshift of the CT bands with respect to those of **L1**. Absorption experiments showed that complexes **1**–**3** absorb much more than both the triflate-substituted cluster precursors and the free ligands **L1**. This increase in absorption, which was not observed for $Pb^{2+}$·**L1** complex, is attributed to an intensity-stealing mechanism induced by vibronic coupling between the CT band of the ligands and $[Mo_6X^i_8]^{4+}$ cluster-based transitions. Owing to the intrinsic abilities of TTF moieties for π-π stacking, **1**–**3** constitute relevant building blocks for the elaboration of a metal-conducting organic framework.

## Experimental Section

**Synthesis of L1 and $[Mo_6X_8(L1)_6](OSO_2CF_3)_4$ Clusters [X = Cl (1), Br (2), and I (3)]:** All the commercial compounds were purchased from Aldrich or Acros. **L1** was prepared according to the literature procedure.[12] $[((n\text{-}C_4H_9)_4N)_2Mo_6X^i_8(OSO_2CF_3)^a_6]$ precursors were prepared for X = Cl, Br, I from solid-state inorganic compounds according to the literature procedure.[10,11] Then, **L1** (X = Cl, 0.126 g, 0.415 mmol; X = Br, 0.0756 g, 0.247 mmol; X = I, 0.066 g, 0.215 mmol) was added to a hot solution of THF (25 mL) containing $[((n\text{-}C_4H_9)_4N)_2Mo_6X^i_8(OSO_2CF_3)^a_6]$ (X = Cl, 0.15 g, 0.0669 mmol; X = Br, 0.10 g, 0.0386 mmol; X = I, 0.10 g, 0.0336 mmol), resulting in an immediate color change from orange to violet. After 5 d of reaction at 80 °C, the mixture was cooled to room temperature (r.t.), filtered, dried under vacuum, then the crude product was washed several times with dry $Et_2O$ until the ether layer became colorless. Finally the crude product was washed with $Et_2O/CH_2Cl_2$ mixture (1:1) and dried under vacuum to obtain analytically pure **1**–**3**. Compounds **1**–**3** are soluble in THF, acetone, DMSO and DMF but are very air-sensitive.

**$[Mo_6Cl_8(L1)_6](OSO_2CF_3)_4$ (1):** IR (KBr): $\tilde{\nu}$ = 3428 (m), 3054 (w), 2875 (m), 1637 (m), 1602 (vs), 1496 (s), 1305 (m), 1221 (s), 1166

  

(s), 1025 (s), 815 (w), 796 (w), 635 (w), 539 (s), 521 (w) $cm^{-1}$. $^1H$ NMR ($CD_3COCD_3$): $\delta$ = 6.67 (s) and 6.72 (s) for 2 H, TTF-CH, 7.39 (s, 1 H, TTF-CH), 7.94 (s, 1 H, CH), 7.99 (s, 1 H, CH), 8.32 (d, 2 H, Py), 8.96 (d, 2 H, Py) ppm. $^{19}F$ NMR ($CD_3COCD_3$): $\delta$ = –79.4 ppm. $^1H$–$^{13}C$ HMQC NMR ($CD_3COCD_3$): 142.1 (C1), 131.4 (C5), 125.3 (C4), 123.4 (C2), 119.6 (C10, C11) ppm. $^1H$–$^{13}C$ HMBC NMR ($CD_3COCD_3$): 154.2 (C3), 134.9 (C6), 114.7 (C6), 105.7 (C8) ppm. $^1H$–$^{15}N$ HMBC NMR ($CD_3COCD_3$): $\delta$ = –179.8 ppm.

**$[Mo_6Br_8(L1)_6](OSO_2CF_3)_4$ (2):** IR (KBr): $\tilde{\nu}$ = 3445 (w), 3054 (w), 2876 (m), 1636 (m), 1604 (vs), 1496 (s), 1305 (m), 1222 (vs), 1163 (s), 1026 (vs), 952 (w), 868 (w), 815 (w), 777 (w), 636 (s), 575 (w), 516 (w) $cm^{-1}$. $^1H$ NMR ($CD_3COCD_3$): $\delta$ = 6.65 (s) and 6.73 (s) for 2 H, TTF-CH, 7.38 (s, 1 H, TTF-CH), 7.90 (s, 1 H, CH), 7.98 (s, 1 H, CH), 8.28 (d, 2 H, Py), 8.94 (d, 2 H, Py) ppm. $^{19}F$ NMR ($CD_3COCD_3$): $\delta$ = –79.3 ppm.

**$[Mo_6I_8(L1)_6](OSO_2CF_3)_4$ (3):** IR (KBr): $\tilde{\nu}$ = 3454 (w), 3054 (w), 2854 (w), 1638 (m), 1603 (vs), 1496 (m), 1220 (s), 1166 (s), 1024 (vs), 952 (w), 867 (w), 815 (w), 636 (s), 538 (w) $cm^{-1}$. $^1H$ NMR ($CD_3COCD_3$): $\delta$ = 6.65 (s) and 6.73 (s) for 2 H, TTF-CH, 7.38 (s, 1 H, TTF-CH), 7.90 (s, 1 H, CH), 7.98 (s, 1 H, CH), 8.28 (d, 2 H, Py), 8.94 (d, 2 H, Py) ppm. $^{19}F$ NMR ($CD_3COCD_3$): $\delta$ = –79.3 ppm.

**Instrumentation:** All experiments were carried out under purified argon using standard Schlenk techniques. All solvents were dried and deoxygenated by standard methods prior to use. The NMR measurements ($^1H$, $^{13}C\{^1H\}$, $^{19}F$, and $^{15}N\{^1H\}$) were carried out with a Bruker Avance (300 and 500 MHz) spectrometer at room temperature. Complete assignment was achieved by use of HMBC and HMQC experiments. The peak positions are reported with positive shifts (ppm) downfield of TMS as calculated from the residual solvent peaks ($^1H$ and $^{13}C\{^1H\}$). Cyclic voltammetry measurements were carried out with a Potentiostat eDAQ instrument. A single-compartment metric cell was equipped with a platinum working electrode, a platinum wire auxiliary electrode, and a SCE reference. The experiments for **L1** and **1**–**3** were performed using ($n$-$Bu_4N$)$PF_6$ as supporting electrolyte in degassed dry THF, under argon at room temperature. IR spectra were recorded on KBr pellets with a Bruker Equinox 55 FTIR spectrometer. UV/Vis absorption measurements were performed on a Varian Cary 5000 UV/Vis/NIR spectrophotometer.

**DFT Calculations:** DFT calculations were performed with the Amsterdam Density Functional package (ADF 2006)[22] on the free ligand **L1** and complex **1**. The geometries were fully optimized without constraints ($C_1$ symmetry). Electron correlation was treated within the local density approximation (LDA) in the Vosko–Wilk–Nusair parametrization.[23] The nonlocal corrections of Becke and Perdew were added to the exchange and correlation energies, respectively.[24] The analytical gradient method implemented by Verluis and Ziegler was used.[25] For the free ligand **L1**, a triple-ξ Slater-type orbital (STO) basis set was used for the valence orbitals of H, C, N, and S, augmented with a 2p single-ξ polarization function for H and a 3d single-ξ polarization function for C, N, and S. To reduce computational effort for complex **1**, a double-ξ STO basis set was used for the valence orbitals of H, C, N, S, and Cl augmented with a 2p single-ξ polarization function for H and a 3d single-ξ polarization function for C, N, S, and Cl. A single-ξ STO basis set was used for 3d orbitals and a triple-ξ STO basis set was used for the valence orbital of Mo augmented with a 5p single-ξ polarization function for Mo. Orbitals up to 1s were kept frozen for C and N, up to 2p were kept frozen for S and Cl, and up to 4p were kept frozen for Mo. The excitation energies and oscillator strengths were calculated following the procedure described by van Gisbergen and co-workers.[26]

**Supporting Information** (see also the footnote on the first page of this article): $^1H$ NMR data (aromatic part) of **1**, **2**, and **3** in $CD_3COCD_3$.

## Acknowledgments

G. P. thanks the Centre National de la Recherche Scientifique (CNRS) for a post-doctoral research grant. Fondation Langlois is acknowledged for financial support.

[1] a) H. Kobayashi, H.-B. Cui, A. Kobayashi, *Chem. Rev.* **2004**, *104*, 5265–5288; b) A. Kobayashi, E. Fujiwara, H. Kobayashi, *Chem. Rev.* **2004**, *104*, 5243–5264; c) E. Coronado, P. Day, *Chem. Rev.* **2004**, *104*, 5419–5448; d) T. Enoki, A. Miyazaki, *Chem. Rev.* **2004**, *104*, 5449–5477.

[2] a) E. J. Welch, J. R. Long, *Prog. Inorg. Chem.* **2005**, *54*, 1–45; b) S. Cordier, K. Kirakci, D. Méry, C. Perrin, D. Astruc, *Inorg. Chim. Acta* **2006**, *359*, 1705–1709.

[3] a) J. C. Sheldon, *J. Chem. Soc.* **1962**, 410–414; b) M. Potel, C. Perrin, A. Perrin, M. Sergent, *Mater. Res. Bull.* **1986**, *21*, 1239–1245; c) N. Prokopuk, D. F. Shriver, *Adv. Inorg. Chem.* **1999**, *46*, 1–49; d) S. Boeschen, H. L. Keller, *Z. Kristallogr.* **1992**, *200*, 305–315; e) A. Peppenhorst, H. L. Keller, *Z. Anorg. Allg. Chem.* **1996**, *622*, 663–669; f) A. Flemstrom, S. Lidin, *Z. Kristallogr.* **2001**, *216*, 41–41.

[4] a) F. Grasset, F. Dorson, S. Cordier, Y. Molard, C. Perrin, A.-M. Marie, T. Sasaki, H. Haneda, M. Mortier, *Adv. Mater.* **2008**, *20*, 143–148; b) F. Grasset, Y. Molard, S. Cordier, F. Dorson, M. Mortier, C. Perrin, M. Guilloux-Viry, T. Sasaki, H. Haneda, *Adv. Mater.* **2008**, *20*, 1710–1715; c) F. Grasset, F. Dorson, Y. Molard, S. Cordier, V. Demange, C. Perrin, V. Marchi-Artzner, H. Haneda, *Chem. Commun.* **2008**, 4729–4731.

[5] a) P. Nanneli, B. P. Block, *Inorg. Chem.* **1968**, *7*, 2423–2426; b) L. Szczepura, K. A. Ketcham, B. A. Ooro, J. A. Edwards, J. N. Templeton, D. L. Cedeno, A. J. Jircitano, *Inorg. Chem.* **2008**, *47*, 7271–7278; c) L. F. Szczepura, B. A. Ooro, S. R. Wilson, *J. Chem. Soc., Dalton Trans.* **2002**, 3112–3116; d) N. Prokopuk, S. Weinert, D. P. Siska, C. L. Stern, D. F. Shriver, *Angew. Chem. Int. Ed.* **2000**, *39*, 3312–3315; e) C. B. Gorman, W. Y. Su, H. W. Jiang, C. M. Watson, P. Boyle, *Chem. Commun.* **1999**, 877; f) G. M. Ehrlich, H. Deng, L. Hill, M. L. Steiger Wald, P. J. Squattrito, F. J. DiSalvo, *Inorg. Chem.* **1995**, *34*, 2480–2482; g) T. Yamagata, H. Okiyama, H. Imoto, T. Saito, *Acta Crystallogr., Sect. C* **1997**, *53*, 859–862; h) T. Saito, N. Massakazu, T. Yamagata, Y. Yamagata, Y. Yamagushi, *Inorg. Chem.* **1986**, *25*, 1111–1117.

[6] a) L. Ouahab, T. Enoki, *Eur. J. Inorg. Chem.* **2004**, 933–941; b) L. Ouahab, E. Yagubskii (Eds.), *Organic Conductors, Superconductors and Magnets: From Synthesis to Molecular Electronics*, NATO Series, Kluwer, Dordrecht, The Netherlands, **2003**.

[7] a) J. Becher, A. Hazell, C. J. McKenzie, C. Vestergaard, *Polyhedron* **2000**, *19*, 665–672; b) F. Iwahori, S. Golhen, L. Ouahab, R. Carlier, J.-P. Sutter, *Inorg. Chem.* **2001**, *40*, 6541–6542; c) S.-X. Liu, S. Dolder, M. Pilkington, S. Decurtins, *J. Org. Chem.* **2002**, *67*, 3160–3162; d) L. Ouahab, F. Iwahori, S. Golhen, R. Carlier, J.-P. Sutter, *Synth. Met.* **2003**, *133–134*, 505–507; e) F. Setifi, L. Ouahab, S. Golhen, Y. Yoshida, G. Saito, *Inorg. Chem.* **2003**, *42*, 1791–1793; f) S. Bouguessa, A. K. Gouasmia, S. Golhen, L. Ouahab, J.-M. Fabre, *Tetrahedron Lett.* **2003**, *44*, 9275–9278; g) S.-X. Liu, S. Dolder, E. B. Rusanov, H. Stoeckli-Evans, S. Decurtins, *C. R. Chim.* **2003**, *6*, 657; h) C. Jia, D. Zhang, Y. Xu, W. Xu, H. Hu, D. Zhu, *Synth. Met.* **2003**, *132*, 249; i) C. Jia, D. Zhang, Y. Xu, W. Xu, D. Zhu, *Synth. Met.* **2003**, *137*, 979; j) S.-X. Liu, S. Dolder, P. Franz, A. Neels, H. Stoeckli-Evans, S. Decurtins, *Inorg. Chem.* **2003**, *42*, 4801–

  

4803; k) T. Devic, N. Avarvari, P. Batail, *Chem. Eur. J.* **2004**, *10*, 3697–3707; l) A. Ota, L. Ouahab, S. Golhen, O. Cador, Y. Yoshida, G. Saito, *New J. Chem.* **2005**, *29*, 1135–1140; m) H. Xue, X.-J. Tang, L.-Z. Wu, L.-P. Zhang, C.-H. Tung, *J. Org. Chem.* **2005**, *70*, 9727–9734; n) N. Benbellat, Y. Le Gal, S. Golhen, A. Gouasmia, L. Ouahab, J.-M. Fabre, *Eur. J. Org. Chem.* **2006**, 4237–4241; o) see also ref.[5] and references given therein.

[8] K. Hervé, S.-X. Liu, O. Cador, S. Golhen, Y. Le Gal, A. Bousseksou, H. Stoeckli-Evans, S. Decurtins, L. Ouahab, *Eur. J. Inorg. Chem.* **2006**, 3498–3502.

[9] a) K. S. Gavrilenko, Y. Le Gal, O. Cador, S. Golhen, L. Ouahab, *Chem. Commun.* **2007**, 280–282; b) N. Benbellat, K. S. Gavrilenko, Y. Le Gal, O. Cador, S. Golhen, A. Gouasmia, J.-M. Fabre, L. Ouahab, *Inorg. Chem.* **2006**, *45*, 10440–10442.

[10] K. Kirakci, S. Cordier, C. Perrin, *Z. Anorg. Allg. Chem.* **2005**, *631*, 411–416.

[11] a) D. H. Johnston, D. C. Gaswick, M. C. Lonergan, C. L. Stern, D. F. Shriver, *Inorg. Chem.* **1992**, *31*, 1869–1873; b) D. Méry, L. Plault, C. Ornelas, J. Ruiz, S. Nlate, D. Astruc, J.-C. Blais, J. Rodrigues, S. Cordier, K. Kirakci, C. Perrin, *Inorg. Chem.* **2006**, *45*, 1156–1167.

[12] R. Andreu, I. Malfant, P. G. Lacroix, P. Cassoux, *Eur. J. Org. Chem.* **2000**, 737–741.

[13] a) L. Pazderski, E. Szlyk, J. Sitowski, B. Kamienski, L. Kozerski, J. Tousek, R. Marek, *Magn. Reson. Chem.* **2006**, *44*, 163–170; b) L. Pazderski, J. Tousek, J. Sitowski, L. Kozerski, R. Marek, E. Szlyk, *Magn. Reson. Chem.* **2007**, *45*, 24–36.

[14] M. Chahma, N. Hassan, A. Alberola, H. Stoeckli-Evans, M. Pilkington, *Inorg. Chem.* **2007**, *46*, 3807–3809.

[15] E. Isomura, K.-I. Tokuyama, T. Nishinaga, M. Iyoda, *Tetrahedron Lett.* **2007**, *48*, 5895–5898.

[16] C. Couldwell, K. Prout, *Acta Crystallogr., Sect. B* **1982**, *38*, 759–765.

[17] For a discussion on the electronic structure of octahedral $M_6X^i_8X_6$ clusters, see for example: a) T. Hughbanks, R. Hoffmann, *J. Am. Chem. Soc.* **1983**, *105*, 1150–1162; b) A. Le Beuze, P. Lamande, R. Lissillour, H. Chermette, *Phys. Rev. B* **1985**, *31*, 5094–5105; c) R. L. Johnston, D. M. P. Mingos, *Inorg. Chem.* **1986**, *25*, 1661–1671; d) T. Hughbanks, *Prog. Solid State Chem.* **1989**, *19*, 329–372; e) L. M. Robinson, R. L. Bain, D. F. Shriver, D. E. Ellis, *Inorg. Chem.* **1995**, *34*, 5588–5596; f) Z. Lin, I. D. Williams, *Polyhedron* **1996**, *15*, 3277–3287; g) R. Gautier, E. Furet, J.-F. Halet, Z. Lin, J.-Y. Saillard, Z. Xu, *Inorg. Chem.* **2002**, *41*, 796–804; h) V. I. Baranovski, D. V. Korolkov, *Int. J. Quantum Chem.* **2004**, *100*, 343–351; i) R. Ramirez-Tagle, R. Arratia-Perez, *Chem. Phys. Lett.* **2008**, *460*, 438–441.

[18] S. Cordier, F. Dorson, Y. Molard, M. Mortier, C. Perrin, B. Fontaine, K. Costuas, R. Gautier, J.-F. Halet, unpublished results.

[19] N. Prokopuk, D. F. Shriver, *Inorg. Chem.* **1997**, *36*, 5609–5613.

[20] D. H. Johnston, C. L. Stern, D. F. Shriver, *Inorg. Chem.* **1993**, *32*, 5170–5175.

[21] a) M. Yuan, B. Ulgüt, M. Mc Guire, K. Takada, F. J. Di Salvo, S. Lee, H. Abruna, *Chem. Mater.* **2006**, *18*, 4296–4306; b) S. Perruchas, N. Avarvari, D. Rondeau, E. Levillain, P. Batail, *Inorg. Chem.* **2005**, *44*, 3459–3465.

[22] a) G. te Velde, F. M. Bickelhaupt, C. Fonseca Guerra, S. J. A. van Gisbergen, E. J. Baerends, J. G. Snijders, T. Ziegler, *J. Comput. Chem.* **2001**, *22*, 931–967; b) C. Fonseca Guerra, J. G. Snijders, G. te Velde, E. J. Baerends, *Theor. Chem. Acc.* **1998**, *99*, 391–403; c) Amsterdam Density Functional program, ADF2005, SCM, Theoretical Chemistry, Vrije Universiteit, Amsterdam, The Netherlands, http://www.scm.com.

[23] S. D. Vosko, L. Wilk, M. Nusair, *Can. J. Chem.* **1980**, *58*, 1200–1211.

[24] a) A. D. Becke, *Phys. Rev. A* **1988**, *38*, 3098–3100; b) J. P. Perdew, *Phys. Rev. B* **1986**, *33*, 8822–8824.

[25] L. Versluis, T. Ziegler, *J. Chem. Phys.* **1988**, *88*, 322–328.

[26] S. J. A. van Gisbergen, J. G. Snijders, E. J. Baerends, *Comput. Phys. Commun.* **1999**, *118*, 119–138.

Received: February 4, 2009
Published Online: March 25, 2009

  